Measurements and Modeling of Stress in Precipitation-Hardened Aluminum Alloy AA2618 during Gleeble Interrupted Quenching and Constrained Cooling

NICOLAS CHOBAUT, DENIS CARRON, PETER SAELZLE, and JEAN-MARIE DREZET

Solutionizing and quenching are the key steps in the fabrication of heat-treatable aluminum parts such as AA2618 compressor impellers for turbochargers as they highly impact the mechanical characteristics of the product. In particular, quenching induces residual stresses that can cause unacceptable distortions during machining and unfavorable stresses in service. Predicting and controlling stress generation during quenching of large AA2618 forgings are therefore of particular interest. Since possible precipitation during quenching may affect the local yield strength of the material and thus impact the level of macroscale residual stresses, consideration of this phenomenon is required. A material model accounting for precipitation in a simple but realistic way is presented. Instead of modeling precipitation that occurs during quenching, the model parameters are identified using a limited number of tensile tests achieved after representative interrupted cooling paths in a Gleeble machine. This material model is presented, calibrated, and validated against constrained coolings in a Gleeble blocked-jaws configuration. Applications of this model are FE computations of stress generation during quenching of large AA2618 forgings for compressor impellers.

DOI: 10.1007/s11661-016-3724-z

I. INTRODUCTION

TO obtain the required mechanical properties, solutionizing and quenching of heat-treatable aluminum alloys (AA) are the key steps. After solutionizing and perfect quenching, a supersaturated solid solution is desired so that during aging elements in solid solution aggregate into fine hardening precipitates and thus increase yield strength. Fast quenching is necessary to avoid any coarse precipitation that would reduce the mechanical properties after heat treatment. However, fast quenching causes also residual stresses (RS) in the part because of its inhomogeneous temperature distribution. In general, it can be said, the thicker the part the more pronounced this effect. As a result, these RS lead to distortions in thick products during machining at final temper,[1] and even in quenched plates, where RS is reduced by a factor ~10 after stress relief.[2] This applies also to large hot-forged parts of AA2618 that are heat treated and then machined to produce impellers.

In Al-Cu-Mg-based alloys, two types of precipitation may take place during quenching and affect the formation of internal stresses. A first precipitation occurs at intermediate temperature (688 K to 573 K (415 °C to 300 °C)[3]) for low cooling rates. The large precipitates are undesirable since they do not harden the material significantly while reducing the amount of elements in solid solution. A second precipitation occurs at lower temperature (below 573 K to 523 K (300 °C to 250 °C)[4]) even for high cooling rates. The resulting effect of these two types of precipitation is an increase of the yield strength and thus of the residual stresses at the surface of large quenched components.[5] For the prediction of RS after quenching, it is thus important to characterize the mechanical properties during cooling by considering possible precipitation. Bibliographical reviews of the finite element (FE) methods applied to the simulation of quenching are given by Mackerle[6] and by Robinson *et al.*[7] The general approach to take into account precipitation is to use yield strength and strain-hardening models where the flow stress depends on the precipitation state.[8–10] Such models require an extensive mechanical characterization of the influence of precipitation on flow stress.[11] Alternatively, Reich and Kessler[12] used their own model with four hardening parameters dependent on the cooling rates and quenching finish temperatures but without viscous effects. Instead, a simpler approach to take into account

NICOLAS CHOBAUT, Scientist, and JEAN-MARIE DREZET, Senior Scientist, are with the Ecole Polytechnique Fédérale de Lausanne, Laboratoire de Simulation des Matériaux, Station 12, 1015 Lausanne, Switzerland. Contact email: jean-marie.drezet@epfl.ch DENIS CARRON, Associate Professor, is with the Univ. Bretagne Sud, FRE CNRS 3744, IRDL, 56100 Lorient, France. PETER SAELZLE, Engineer, is with ABB Turbo Systems Ltd, Bruggerstrasse 71a, 5400 Baden, Switzerland.

Manuscript submitted April 7, 2016.
Article published online August 29, 2016

precipitation in a very simplified way was used in Reference 13 for the modeling of the as-quenched RS in thick aluminum alloys plates. It consists of a thermo-mechanical model whose parameters are identified using a limited number of tensile tests achieved after representative interrupted cooling paths in a Gleeble machine. This approach referred to as "TMG model" in the following is used in this paper. TMG stands for thermo-mechanical model using Gleeble tests.

The mechanical data available in the literature are usually not representative of quenching conditions since they are obtained after heating from room temperature to the desired temperature. Interrupted quench tests from the solutionizing temperature, *i.e.*, from a solid solution at equilibrium without precipitates, are required. Such tests performed on AA6082 and AA7020,[12] AA7040 and AA7449[13] and AA7010[11] were used in the literature to feed material models for RS prediction. The mechanical properties obtained with such tests are used to feed finite element (FE) simulations of unconstrained quenching. The accuracy of such simulations depends on the thermal field and thereby on the precipitation state assuming that the Bauschinger effect due to nonmonotonic loading during quenching is negligible.

In the present study, the mechanical properties of the AA2618 alloy deduced from Gleeble interrupted quench tests are validated using constrained cooling (CC) experiments performed in the Gleeble machine. In other words, the material model determined in isothermal conditions is validated in nonisothermal conditions. The test consists in cooling a tensile specimen from the solutionizing temperature in the thermo-mechanical simulator while keeping both extremities blocked by fixed jaws. Compared to unconstrained cooling conditions, this so-called "blocked-jaws test" creates tensile stresses in the specimen which cannot contract. Such tests are similar upon cooling to Satoh tests[14] used to characterize the phase changes in steels and also in aluminum alloys by Zhang *et al.*[15] As long as the cooling of the specimen takes place predominantly along its axis, *i.e., via* the jaws, the test is readily simulated by imposing the measured axial temperature profile in the FE model. Measured stress and strain evolutions during cooling are then compared with the computed results.

The interrupted quench (IQ) tests used to characterize the mechanical behavior of AA2618 upon cooling are shown in this paper. The model parameters determined using these IQ tests are used in two numerical thermo-mechanical models to simulate the blocked-jaws tests:

- TM model: Thermo-mechanical model ignoring precipitation and
- TMG model: Thermo-mechanical model accounting for precipitation in a simple but realistic way. Instead of modeling precipitation that occurs during quenching, it is accounted for directly in the constitutive equation. The model parameters are identified using a limited number of tensile tests achieved after representative interrupted cooling paths in a Gleeble machine.

II. EXPERIMENTAL PROCEDURE

The probe material for the tensile tests in the Gleeble machine was taken form AA2618 forgings for impellers in turbochargers (Al-2.4 Cu-1.55 Mg-1.1 Ni-1.1 Fe, wt pct) with an average grain size of 40 μm. The specimens were presolutionized in a furnace for 4 hours at 803 K (530 °C) – the solutionizing temperature – quenched in cold water and stored in a freezer at ca. 263 K (−10 °C) to retard any precipitation.

The Gleeble 3500 machine was selected for its precise temperature control[13] in order to perform IQ tests and constrained coolings. Specimens are heated by Joule effect from room temperature to the solutionizing temperature at 30 K/s. The force is maintained near zero to allow for free dilatation (zero force control) during heating and solutionizing in the Gleeble.

A. *Interrupted Quench Tests*

For IQ tests, specimens are isothermally tensile tested after being cooled at zero force control from the solutionizing temperature with either

- "IQ1": fast interrupted quench in order to characterize the solid solution without precipitates or
- "IQ2": interrupted quench with a cooling rate of 20 K/s above 573 K (300 °C), *i.e.*, much faster than in the real forgings, to avoid coarse S/S' precipitation.[3] Between 523 K (250 °C) and 423 K (150 °C) where precipitation hardening occurs,[4] "IQ2" features cooling rates close to the surface cooling rates measured in forgings.

The tests "IQ1" and "IQ2" allow identifying the parameters of the constitutive law used for the TM and TMG models, respectively.

B. *Constrained Coolings*

In constrained coolings, three different cooling conditions from the solutionizing temperature are imposed in the Gleeble machine:

- "CC1": constrained cooling representative of boiling water quenching of a large forging, with a typical temperature plateau around 373 K (100 °C).
- "CC2": constrained cooling faster than 20 K/s above 573 K (300 °C) to avoid S/S' phase formation and fast below 423 K (150 °C) without "CC2a" or with "CC2b" air cooling.
- "CC3": constrained cooling slightly faster than "CC1" above 423 K (150 °C) and as fast as possible without additional air/water below 423 K (150 °C).

"CC1" is representative of industrial practice, "CC2-b" is close to "IQ2" used to feed the TMG model, and "CC3" is intermediate between "CC1" and "CC2." Except for "CC2b" which uses additional air cooling, all coolings are achieved by heat extraction *via* the copper grips, *i.e.* along the specimen axis as mentioned in the introduction.

As coolings are performed using a blocked-jaws configuration (stroke imposed to zero), the specimens

undergo thermal contraction but are constrained, thus leading to the build-up of tensile axial stresses.

For IQ and constrained cooling tests, an optimized geometry was designed (Figure 1) to localize deformation at the mid-length of the specimen, where the cross section is minimal. A diametral extensometer is used to monitor strain during the test.

It is carefully positioned at the very center of the specimen, *i.e.*, at the center of the gage length. The hoop strain and axial stress at this location are calculated using

$$\varepsilon_{\theta\theta} = \ln\left[\frac{d}{d_0}\right] \text{ and } \sigma_{zz} = \frac{F}{(\pi d^2/4)}, \quad [1]$$

where d_0 is the diameter at the start of cooling, *i.e.*, at the end of the solutionizing and F is the measured force.

Specimens are equipped with three thermocouples and an additional thermocouple (TC4) positioned at 27 mm from TC1 in order to estimate the axial thermal gradient.

III. MODELING

A. *Thermo-Mechanical Behavior*

To fit the stress–strain curves measured in the interrupted quench tests, an elasto-viscoplastic constitutive law with additive hardening (Chaboche-type model) is chosen.[16] The procedure applied in Reference 13 to the quench-sensitive AA7449 alloy is detailed hereafter.

The uniaxial tensile load at constant temperature is defined by

$$\sigma_{zz} = \sigma_y + H(p_{cum})^n + K(\dot{p})^m \text{ with } \dot{p} = \left|\dot{\varepsilon}^{in}_{zz}\right| \text{ and } p_{cum} = \int_{T<T_{cum}} \dot{p}dt, \quad [1]$$

where σ_{zz} is the axial flow stress, $\dot{\varepsilon}^{in}_{zz}$ is the inelastic strain rate, and p_{cum} is the inelastic deformation accumulated below T_{cum}. This temperature corresponds to the temperature above which inelastic deformation has no effect on the subsequent low-temperature behavior. It represents a simple way to consider plastic strain recovery at high temperature.[13] In Eq. [2], σ_y is the yield strength at 0 pct strain offset, H and n are hardening parameters, K is the consistency, and m is the strain-rate sensitivity. Precipitation mainly affects σ_y,[17] which depends on the nature, size, and volume fraction of precipitates as well as on solute concentration in the matrix, see for instance Reference 18. Although the parameters of the additive law in Eq. [2] are slightly more difficult to identify than the parameters of multiplicative laws,[16] Eq. [2] has the advantage to allow a direct calibration of a yield strength model that predicts σ_y.[5]

The temperature-dependent parameters (H, n, K, m) are considered independent of precipitation as checked experimentally.[19] These parameter values are therefore identical for the TM and the TMG models. Hence the models differ only by σ_y values. Using the stress–strain curves achieved after IQ tests, σ_y yield strength values are determined in order to be used in the TM and TMG models. The TM model ignoring precipitation is fed by σ_y values after "IQ1" coolings corresponding to a state as close as possible to supersaturated solid solution. The TMG model uses σ_y values obtained through tensile tests after slower "IQ2" coolings where precipitation hardening by cluster formation occurs below 573 K (300 °C).[4]

In the constitutive law (Eq. [2]), the temperature-dependent parameters (σ_y, H, n, K, m) are interpolated linearly as a function of temperature.

B. *Mechanical Model of Constrained Cooling*

Instead of simulating the transient temperature evolution with the help of a thermo-electrical simulation,[20–22] it is chosen to impose a thermal field history for the stress–strain analysis. As aluminum alloys are highly conductive, the specimen diameter is rather small and the maximum sample temperature during the test is 803 K (530 °C), the radial thermal gradient can be neglected. Indeed, the Biot number is much lower than 0.1[23] at position of TC1 where the heat lost by natural convection of the air surrounding the specimen is small compared to the heat extracted by conduction *via* the jaws. In this case, temperature depends only on time and position along the specimen axis. The measured temperature profiles during cooling are fitted by a polynomial as shown in Figure 2 and imposed as a thermal loading in the stress–strain computations. Only one

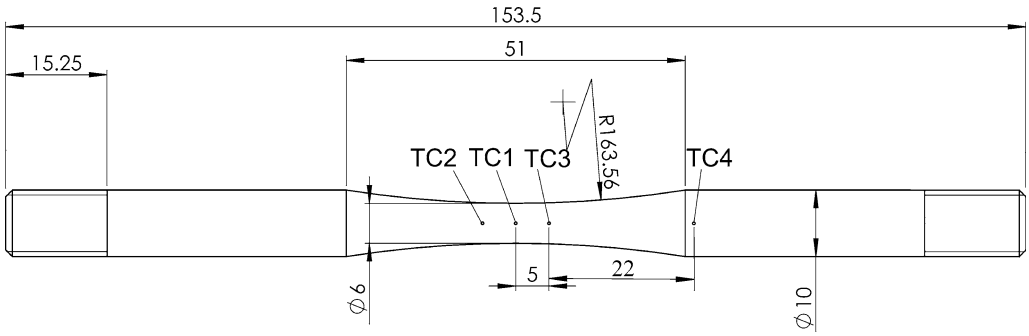

Fig. 1—Specimen geometry used for tensile test in the Gleeble machine (dimensions in millimeters).

polynomial fit was necessary, since the temperature profiles measured for each cooling condition described before were almost identical.

The imposed thermal loading reproduces the cooling from the solutionizing temperature to room temperature as described in Section II–B. The mechanical loading of the Gleeble specimens during cooling with zero stroke displacement is simulated with the Abaqus software using an axisymmetric model with a mesh (Figure 3) made of quadrilateral elements (CAX8). The boundary conditions shown in Figure 3 simulate the zero stroke condition imposed experimentally.

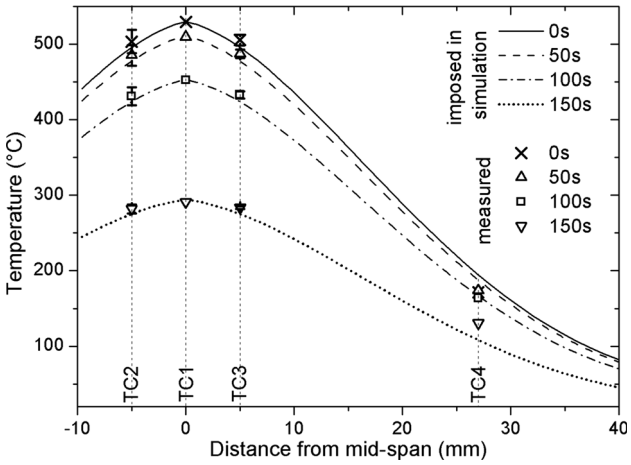

Fig. 2—Imposed temperature profile in stress–strain simulation obtained by a polynomial fit of the measured temperatures.

Fig. 3—Half of specimen modeled in Abaqus using an axisymmetric model together with the imposed mechanical boundary conditions.

Outputs of the FE simulation are the axial stress at the specimen mid-span and the radial displacement at position of TC1 from which the hoop strain is calculated using Eq. [1].

IV. RESULTS AND DISCUSSION

A. *Characterization of Material Properties by Interrupted Quench Test*

The imposed temperature cycles are shown in Figure 4(a) and corresponding stress–strain curves achieved after IQ1 and IQ2 tests are shown in Figure 4(b).

Copper grips and additional air or water cooling were used for interrupted quenches "IQ1." The fastest quench was achieved by water quench (WQ) interrupted at 298 K (25 °C). WQ interrupted at higher temperatures being too challenging due to high overshoots, WQ to 298 K (25 °C) followed by a fast reheat to 373 K (100 °C) or 423 K (150 °C) was performed. Tensile tests at 523 K (250 °C) or 473 K (200 °C) were performed after air quench interrupted at these temperatures.

Copper grips above 423 K (150 °C) and additional air cooling at lower temperatures were used for interrupted quenches "IQ2." These coolings were interrupted at either 773 K (500 °C), 723 K (450 °C), 673 K (400 °C), 623 K (350 °C), 573 K (300 °C), 523 K (250 °C), 473 K (200 °C), 423 K (150 °C) or 308 K (35 °C) where isothermal tensile loads were performed.

At high temperature, the flow stress is strain-rate dependent as shown exemplarily for IQ2 tests at 673 K (400 °C) and 773 K (500 °C). It was checked that strain-rate sensitivity (SRS) is small at and below 573 K (300 °C) but not at 623 K (350 °C) as shown by strain-rate jumps performed at this temperature in Reference 19. For IQ2 tests, flow stress increases during cooling due to the combined effect of temperature decrease and precipitation hardening. For IQ1 tests, the flow stress is the lowest at 308 K (35 °C), increases slightly during the reheat to 373 K (100 °C), and

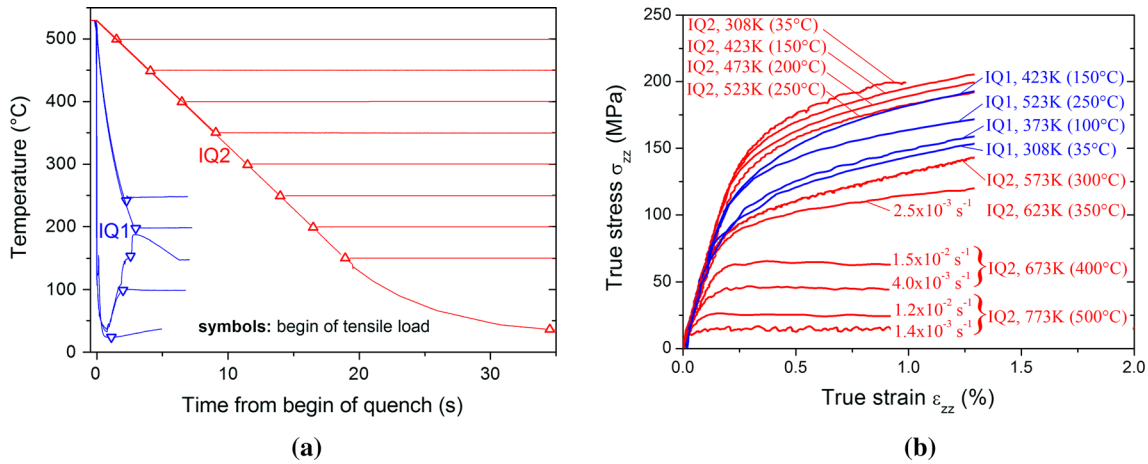

Fig. 4—(*a*) Interrupted quenches and (*b*) corresponding stress–strain curves at constant temperature. Strain rates at and below 573 K (300 °C) are within 0.8 to 1.7 × 10^{-2} s^{-1}.

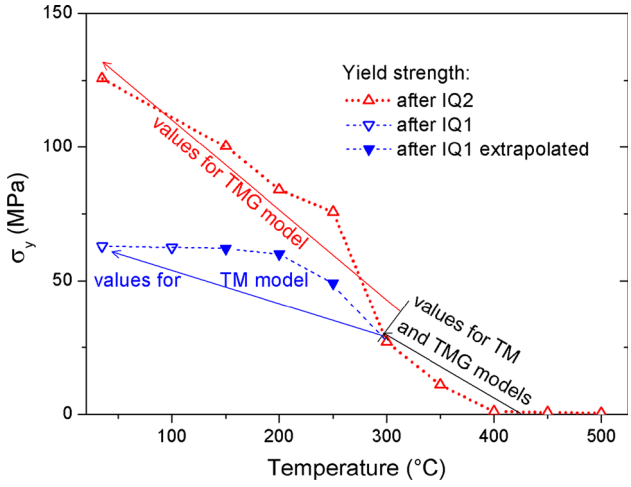

Fig. 5—Yield strength identified from tensile loads at constant temperature after interrupted quenches.

significantly during the reheat to 423 K (150 °C). This is explained by precipitation hardening during reheat from the state as close as possible to supersaturated solid solution obtained by WQ. For a given temperature, flow stress after IQ2 is higher than flow stress after IQ1 because of precipitation hardening below 573 K (300 °C).[4]

The yield strength values σ_y in Figure 5 and the four other model parameters (H, n, K, m) in Figure 6 are determined using the stress–strain curves achieved after IQ tests. The identification procedure by inverse method using a dedicated optimization software (SiDoLo) developed by Pilvin[24] is fully detailed in Reference 19 in particular the extrapolation of σ_y values after "IQ1" (full symbols in Figure 5).

At high temperature, the σ_y values obtained during "IQ2" (Figure 5) are used for the two models, since the volume fraction of S/S' phase formed during cold water quench is low as shown by *in situ* SAXS measurements.[4] In other words, σ_y is considered little affected by high temperature precipitation due to the short time spent at high temperature during quenching. The TM and TMG models differ only from σ_y under 573 K (300 °C). The TM model and TMG model are fed by σ_y values obtained after fast coolings "IQ1" and after slower coolings "IQ2," respectively. The σ_y values obtained after "IQ1" correspond to a state as close as possible to supersaturated solid solution. The fact that the σ_y values obtained after "IQ2" are higher than the ones after "IQ1" below 573 K (300 °C) is attributed to precipitation hardening by cluster formation.[4]

The strain-hardening parameters H and n (Figure 6(a)) are the highest at low temperature due to maximum dislocation storage and decrease with increasing temperature due to dislocation annihilation. At high temperature [≥673 K (400 °C)], where H is set close to zero, n is also set close to zero in accordance with Magnin's results on Al-Cu alloys.[25]

The K-Temperature curve (Figure 6(b)) exhibits the typical bell shape encountered in metallic alloys. K values are low at low temperature (<523 K (250 °C)) where strain-rate sensitivity (SRS) is small but also at high temperature where the viscous stress is limited by the ultimate strength which becomes small. Below 573 K (300 °C), m is set to low values and increases rapidly at higher temperatures. Full symbols indicate the extrapolated K and m values at the solutionizing temperature used for the FE simulations.

B. *Validation of Material Properties Against Constrained Coolings*

The cooling curves and corresponding cooling rates for the three cooling conditions described in Section II–B are shown in Figure 7(a) and (b), respectively.

Above 383 K (110 °C), coolings "CC1" and "CC3" are typical for the slowest and the fastest temperature evolutions measured at the surface of large forgings quenched in boiling water.[26] The coolings differ below 383 K (110 °C). Instead of holding the temperature at 373 K (100 °C), which corresponds to boiling water quenching, cooling "CC3" is fast below 373 K (100 °C) in order to limit precipitation hardening below 373 K (100 °C) compared to cooling condition "CC1." To shorten the experiment duration corresponding to "CC1," the cooling rate below 373 K (100 °C) was increased compared to industrial practice where cooling to room temperature can take up to several hours depending on the size of the forging. Cooling "CC2a" corresponds to the fastest achieved cooling without additional air/water. The cooling rate is higher than 20 K/s in the 473 K to 773 K (200 °C to 500 °C) temperature range and similar to the one of cooling "CC3" below 473 K (200 °C). This cooling condition was chosen to avoid the formation of S/S' phases at high temperature and limit precipitation hardening at low temperature. Cooling "CC2b" is slightly faster than "CC2a" below 423 K (150 °C) due to the additional air cooling.

For the different coolings, the measured axial stress and the hoop strain rate are shown in Figure 8(a) and (b), respectively.

The stress and strain-rate evolutions are almost identical for coolings "CC2a" and "CC2b" above 473 K (200 °C), showing the excellent experimental reproducibility. The slightly higher stress for cooling "CC2a" compared to "CC2b" may be due to precipitation hardening by cluster formation at low temperature. However, the stress difference between the two cooling conditions is within the measurement uncertainty.

Above ca. 688 K (415 °C) – this temperature corresponds to the onset of precipitation detected by differential scanning calorimetry (DSC) in the cooling rate range 0.017 to 1.17 K/s[3] – Figure 8 shows the positive SRS of AA2618: the higher the strain rate, the higher the axial stress. In the 573 K to 688 K (300 °C to 415 °C) temperature range, this strain-rate effect also explains the different stress values between the tests at ca. -7×10^{-5} s^{-1} and the test at ca. -2×10^{-3} s^{-1}.

The two coolings "CC1" and "CC3" exhibit different strain rates below 573 K (300 °C) (Figure 8(b)), whereas stresses are comparable (Figure 8(a)). Thus, the SRS of AA2618 is negligible below 573 K (300 °C) as confirmed in Figure 4(b).

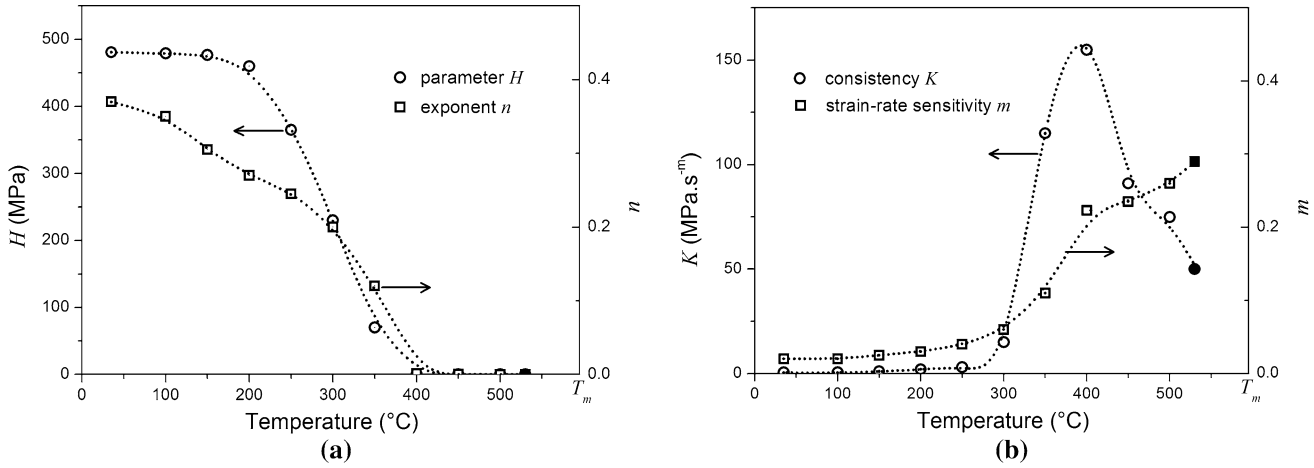

Fig. 6—(*a*) Strain hardening and (*b*) viscous parameters of Eq. [1] for AA2618. Open symbols are identified, full symbols are extrapolated; dashed lines are guides for the eye.

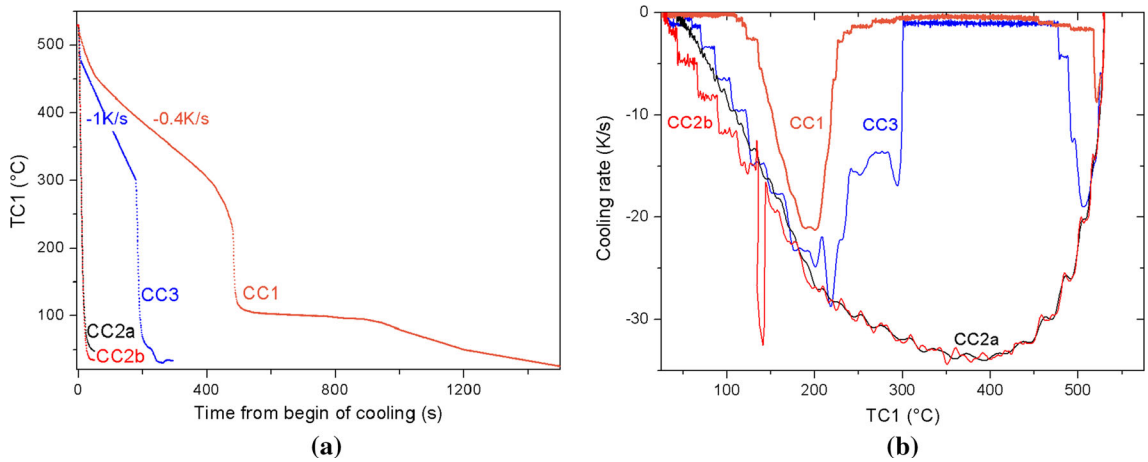

Fig. 7—(*a*) Cooling curves and (*b*) corresponding cooling rates achieved during blocked-jaw tests.

On the other hand, the two coolings "CC2a" and "CC2b" exhibit below 473 K (200 °C) comparable strain rates but slightly different stresses. As SRS is nihil at these temperatures, this stress difference can only be attributed to precipitation hardening as mentioned above.

The stress is higher for coolings "CC2a" and "CC2b" than for cooling "CC3" in the 503 K to 573 K (230 °C to 300 °C) temperature range (Figure 8(a)). This is attributed to the solute loss during coolings "CC1" and "CC3" which decreases solution strengthening and/or decreases the precipitation hardening potential below 573 K (300 °C). Indeed, DSC results on AA2618[3] showed that S/S' phases are avoided during coolings "CC2a" and "CC2b," but form during coolings "CC1" and "CC3."

The stress–temperature curves of coolings "CC1" and "CC3" are almost identical down to 373 K (100 °C). This means the two coolings feature the same thermo-mechanical behavior above 373 K (100 °C). This indicates that the mechanical behavior is identical for these two coolings representative of industrial practice.

The stress increase around 373 K (100 °C) for cooling "CC1" (Figure 8(a)) is attributed to precipitation hardening during the ca. 400 seconds at 373 K (100 °C) (Figure 7(a)). This hardening is lower than the one achieved for coolings "CC2a" and "CC2b" due to the solute lost above 573 K (300 °C) during cooling "CC1" which is not available for precipitation hardening.

Cooling "CC3" provides a stress–temperature curve approaching the lowest one achievable during quenching of AA2618 (Figure 8(a)). Indeed, precipitation hardening is limited by the combination of low cooling rate above 573 K (300 °C) and relatively high cooling rate below 573 K (300 °C).

By avoiding the formation of S/S' phase, coolings "CC2a" and "CC2b" provide a stress–temperature curve close to the maximum hardening achievable during quenching. Below 573 K (300 °C), higher stresses would be reached with a reduced cooling rate that would increase precipitation.

In Figure 9, the measured stress–temperature curves for coolings "CC2a" and "CC2b" are compared to FE simulations using:

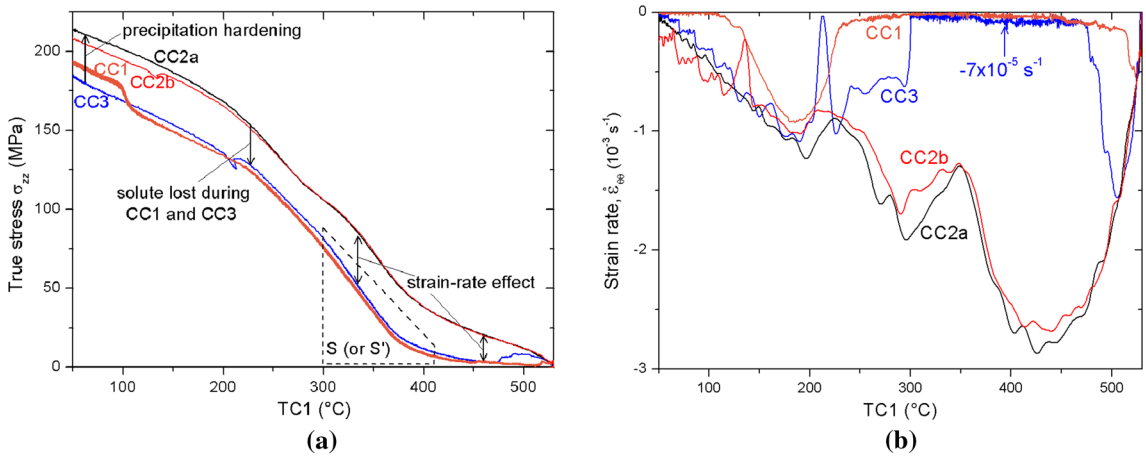

Fig. 8—(*a*) Evolution of measured axial stress and (*b*) hoop strain rate during blocked-jaw tests.

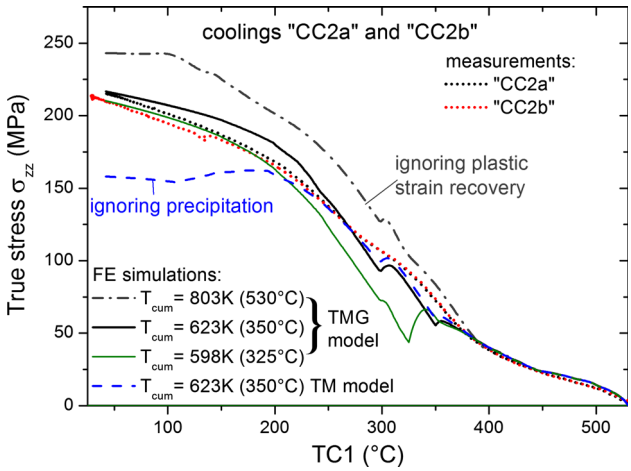

Fig. 9—Comparison between measured and predicted stress evolution during constrained coolings "CC2a" and "CC2b".

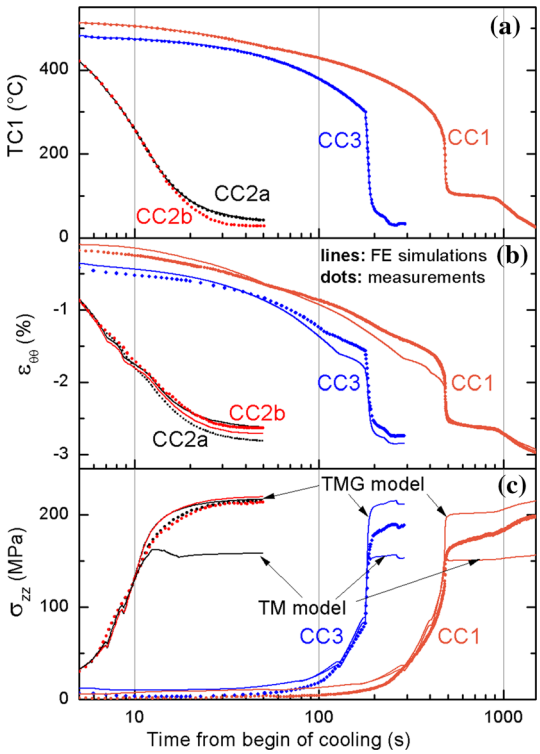

Fig. 10—(*a*) Cooling cycles and comparison between measured (dotted lines) and simulated (solid lines), (*b*) hoop strain, and (*c*) axial stress evolutions. The TM and TMG models give identical strains but different stresses.

- the TMG model ignoring plastic strain recovery at high temperature [T_{cum} = 803 K (530 °C)],
- the TMG model with plastic strain recovery above either 598 K (325 °C) or 623 K (350 °C), and
- the TM model with plastic strain recovery above 623 K (350 °C).

The TMG model predicts stresses in a relatively good agreement with the measurements when 598 K (325 °C) or 623 K (350 °C) are taken for T_{cum}. Nevertheless, some differences between the stresses predicted using these two values of T_{cum} are shown in Figure 9. On the one hand, the value of 623 K (350 °C) instead of 598 K (325 °C) provides a better agreement with the measured stresses between 548 K (275 °C) and 648 K (375 °C). On the other hand, the agreement between 323 K (50 °C) and 473 K (200 °C) is better with a value of 598 K (325 °C) for T_{cum}. At the end of cooling, the residual stresses predicted by the TMG model with plastic strain recovery above either 598 K (325 °C) or 623 K (350 °C) differ only by 2 pct. Ignoring plastic strain recovery (T_{cum} = 803 K (530 °C) in Figure 9), however, leads to RS overestimated by ca. 15 pct compared to the measured RS. The value of 623 K (350 °C) for T_{cum} is chosen for further calculations.

For the three cooling conditions described in Section II–B, the experimental results of blocked-jaw tests are shown in Figure 10, together with the results by FE simulation using the TM and TMG models.

For coolings "CC2a" and "CC2b", Figure 10(c) shows the relatively good agreement between measured stresses and simulated ones using the TMG model, as already shown in Figure 9. The agreement in terms of

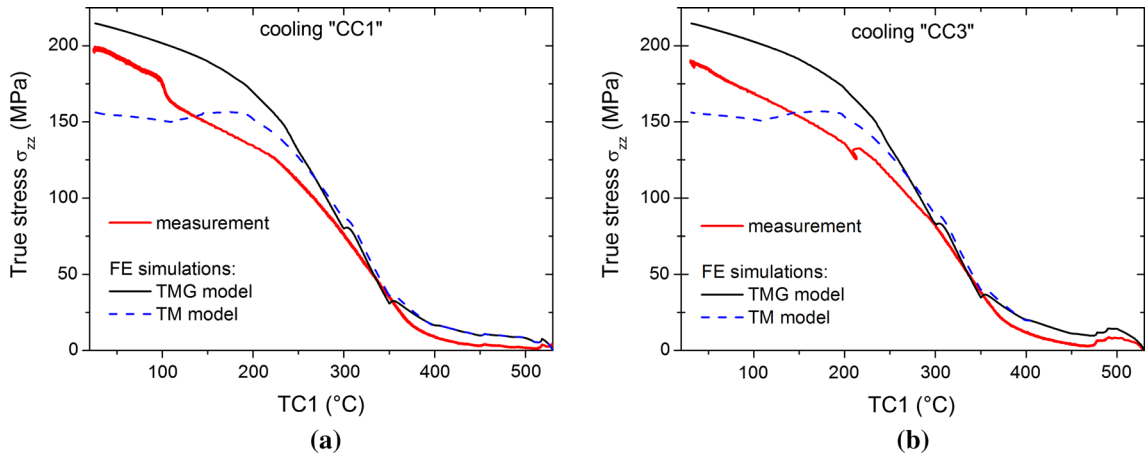

Fig. 11—Stress evolution *vs* temperature during constrained coolings (*a*) "CC1" and (*b*) "CC3." T_{cum} = 623 K (350 °C) for all FE simulations.

strains in Figure 10(b) is excellent for the first 10 seconds and acceptable for longer times considering the uncertainty on strain measurement.

For coolings "CC1" and "CC3," the measured hoop strain evolutions in Figure 10(b) are qualitatively well reproduced by the simulation. In terms of stresses, the agreement between measurements and simulations with the TM or TMG model is good at intermediate temperature [573 K to 623 K (300 °C to 350 °C)] but poor outside of this temperature range as shown in Figure 10(c) and also in Figure 11.

At high temperature [>623 K (350 °C)], the stress predicted by the simulations is slightly higher than the measured one. This may be due to the fact that the model parameters were determined in the 8×10^{-4} to 0.03 s^{-1} axial strain-rate range (*i.e.* -4×10^{-4} to -0.015 s^{-1} hoop strain-rate range). This is higher than the strain rates achieved in the blocked-jaw tests corresponding to coolings "CC1" and "CC3" (Figure 8(b)).

At low temperature [<373 K (100 °C)], the measured stresses are overestimated by the simulations with the TMG model and underestimated by the simulations with the TM model. This is due to the fact that the yield strength values used in the models (Figure 5) are different from the real values during coolings "CC1" and "CC3" as discussed before.

The fact that the TM model underestimates stresses for the three blocked-jaw tests is attributed to precipitation hardening that occurs in the tests but is not taken into account by the TM model. This model ignoring precipitation provides the lower bound, *i.e.*, the stress that would be achieved without precipitation hardening at low temperature. The TMG model provides an upper bound for boiling water quenching of industrial practice, where the cooling rate at high temperature is too slow to avoid S/S' phase formation.

V. CONCLUSION

Interrupted quench tests have been performed to determine the mechanical behavior of AA2618 at different temperatures below its solutionizing temperature. The flow stress of the alloy as close as possible to its supersaturated solid solution was determined after water quench. Below 573 K (300 °C), this flow stress was found to be significantly lower than the one after interrupted quenches after cooling at 20 K/s. The identified model parameters were used to simulate the Gleeble constrained coolings in a blocked-jaws configuration. At high temperature [>573 K (300 °C)], the agreement between constrained cooling measurements and simulation is relatively good with well-simulated strain-rate effects whether the TM or the TMG model is used.

At lower temperature, the agreement between measurements and simulation is good with the TMG model provided that the constrained cooling and the interrupted quenches have a similar cooling rate with an identical thermal history at high temperature.

If this is not the case, as for coolings similar to boiling water quenching of forgings, the simulation using the TM model (resp. TMG model) underestimates (resp. overestimates) the stresses measured during constrained cooling. For unconstrained coolings and assuming that the thermal field is well known, it can be inferred that the TM model will give a lower bound for RS predictions in boiling water-quenched forgings. An upper bound will be given by the TMG model.

The application of the TMG model to the quenching of large AA2618 forgings is described in Reference 26 where model results are compared with residual stress measurements using neutron diffraction.

ACKNOWLEDGMENTS

This work is funded by the Competence Center for Materials Science and Technology in the frame of the project entitled "Measurements and modeling of residual stress during quenching of thick heat-treatable aluminum components in relation to their microstructure" involving EPF Lausanne, PSI Villigen, Univ. Bretagne

Sud Lorient, Constellium and ABB Turbo Systems Ltd. The Gleeble 3500 machine of Univ. BretagneSud was co-financed by European Regional Development Fund. The authors are grateful to Professor P. Pilvin and W. Berckmans (Univ. Bretagne Sud) for providing SiDoLo and for the instrumentation of the Gleeble specimens, respectively.

REFERENCES

1. B. Dubost, M. Bouet-Griffon, P.H. Jeanmart, and M.O. Homette: *Proceedings of the International Conference on Residual Stresses*, Edited by: G. Beck, S. Denis, and A. Simon, Springer, 1989, pp. 581–86.
2. JC Boyer and M Boivin: *Mater. Sci. Technol.*, 1985, vol. 1, pp. 786–92.
3. N Chobaut, D Carron, and J-M Drezet: *J Alloys Compd.*, 2016, vol. 654, pp. 56–62.
4. P Schloth, A Menzel, JL Fife, JN Wagner, H Van Swygenhoven, and J-M Drezet: *Scr. Mater.*, 2015, vol. 108, pp. 56–59.
5. D. Godard, P. Archambault, S. Denis, E. Gautier, and F. Heymes: *Proceedings of the 7th International Seminar of IFHT on Heat Treatment and Surface Engineering of Light Alloys,* Edited by: J. Lendvai and T. Réti, 1999, pp. 249–57.
6. J Mackerle: *Comput. Mater. Sci.*, 2003, vol. 27, pp. 313–332.
7. JS Robinson, DA Tanner, and CE Truman: *Strain*, 2014, vol. 50, pp. 185–207.
8. D Bardel, M Perez, D Nelias, A Deschamps, CR Hutchinson, D Maisonnette, T Chaise, J Garnier, and F Bourlier: *Acta Mater.*, 2014, vol. 62, pp. 129–40.
9. A Deschamps and Y Brechet: *Acta Mater.*, 1998, vol. 47, pp. 293–305.
10. S Gouttebroze, A Mo, Ø Grong, KO Pedersen, and HG Fjær: *Metall. Mater. Trans. A*, 2008, vol. 39, pp. 522–34.
11. D. Godard, P. Archambault, J.-P. Houin, E. Gautier, and F. Heymes: *Proceedings of ICAA6*, Edited by: T. Sato, S. Kumai, T. Kobayashi, and Y. Murakami, 1998, pp. 1033–8.
12. M Reich and O Kessler: *Mater. Sci. Technol.*, 2012, vol. 28, pp. 769–72.
13. N Chobaut, D Carron, S Arsène, P Schloth, and J-M Drezet: *J. Mater. Process. Technol.*, 2015, vol. 222, pp. 373–80.
14. K Satoh: *Trans. Jpn. Weld. Soc.*, 1972, vol. 3, pp. 125–34.
15. ZL Zhang, Ø Gundersen, R Aune, J Ødegård, and Ø Grong: *Comput. Mater. Sci.*, 2005, vol. 34, pp. 35–45.
16. J Lemaître and J-L Chaboche: *Mechanics of Solid Materials*, Cambridge University Press, Cambridge, UK, 1990.
17. S Denis, P Archambault, E Gautier, A Simon, and G Beck: *J. Mater. Eng. Perform.*, 2002, vol. 11, pp. 92–102.
18. OR Myhr, Ø Grong, and SJ Andersen: *Acta Mater.*, 2001, vol. 49, pp. 65–75.
19. N. Chobaut: *EPFL Ph.D. Thesis n°6559, 2015*, DOI: 10.5075/epfl-thesis-6559, http://infoscience.epfl.ch/record/205768/files/EPFL_TH6559.pdf.
20. C Zhang, M Bellet, M Bobadilla, H Shen, and B Liu: *Metall. Mater. Trans. A*, 2010, vol. 41, pp. 2304–17.
21. SGR Brown, JD James, and JA Spittle: *Model. Simul. Mater. Sci. Eng.*, 1997, vol. 5, pp. 539–48.
22. SD Norris and I Wilson: *Model. Simul. Mater. Sci. Eng.*, 1999, vol. 7, pp. 297–309.
23. D.R. Pitts and L.E. Sissom: *Theory and Problems of Heat Transfer*, McGraw_Hill, New York, USA, 1977.
24. P. Pilvin and G. Cailletaud: *Proceedings of the Second International Symposium on Inverse Problems,* Edited by: H.D. Bui, M. Tanaka, M. Bonnet, H. Maigre, E. Luzzato, and M. Reynier, Balkema, 1994, pp. 79–86.
25. B Magnin, L Maenner, L Katgerman, and S Engler: *Mater. Sci. Forum*, 1996, vol. 217, pp. 1209–14.
26. N Chobaut, P Saelzle, G Michel, D Carron, and J-M Drezet: *JOM*, 2015, vol. 67, pp. 984–90.